Electron Nuclear Double Resonance Study of the Mn^{2+} Environs in the Oxalate–ATP Complex of Pyruvate Kinase†

Xiaoling Tan‡

Department of Physics, State University of New York at Albany, Albany, New York 12222

Russell Poyner and George H. Reed

Institute for Enzyme Research, Graduate School, and Department of Biochemistry, College of Agricultural and Life Sciences, University of Wisconsin—Madison, Madison, Wisconsin 53705

Charles P. Scholes*

Department of Chemistry and Center for Biochemistry and Biophysics, State University of New York at Albany, Albany, New York 12222

Received February 11, 1993; Revised Manuscript Received May 14, 1993

ABSTRACT: Electron nuclear double resonance (ENDOR) and the related pulse technique of pulse field sweep EPR (PFSEPR) were used to probe the site I environment of Mn^{2+} in the oxalate–ATP complex of pyruvate kinase. Assignment of features and an estimate of hyperfine couplings have shown proximity of protons to the metal ions through their dipolar interaction and proximity of ^{31}P and ^{17}O because of a contact interaction from direct Mn^{2+}–ligand covalent spin transfer. Since Mn^{2+} is a spin $^5/_2$ ion whose $M_S = \pm^1/_2, \pm^3/_2$, and $\pm^5/_2$ electron spin states can all contribute to EPR and ENDOR, we have developed experimental and theoretical strategies for elucidating hyperfine couplings to the Mn^{2+} electron spin states. Solvent-exchangeable proton ENDOR features were evident with couplings very similar to the hyperfine couplings of H_2O in $[Mn(H_2O)_6]^{2+}$. ENDOR of exchangeable, more distant protons originated from a dipolar coupling such as could be expected from protons residing 5.5 Å from Mn^{2+} and hydrogen-bonded to a nonliganding oxygen or nitrogen. Nonexchangeable proton ENDOR features indicated dipolar coupling to proton(s) from the protein residing at ~4.5 Å from the Mn^{2+}. The ~4-MHz ^{31}P phosphate hyperfine couplings in Mn(II)–nucleotide models and in pyruvate kinase were similar, but a detailed ENDOR and PFSEPR comparison revealed that the hyperfine coupling to the ATP γ-phosphate in pyruvtae kinase was ~10% less than coupling to phosphates of Mn(II)–nucleotides. [In pyruvate kinase only the γ-phosphate has been shown to bind to Mn^{2+} at site I (Lodato & Reed, 1987).] Well-resolved ENDOR features from ^{31}P γ-phosphate of pyruvate kinase and Mn(II)–nucleotide models were observed at a low field, 1150 G below $g = 2.00$, where they showed coupling to the electron $M_S = -^5/_2$ state. The excellent resolution of ^{31}P phosphate ENDOR at this low field was attributed to angle selection due to the proximity of a zero-field splitting axis and a ^{31}P hyperfine axis. ^{17}O couplings from isotopically enriched [γ-^{17}O]ATP and [^{17}O]-oxalate were particularly evident in the outlying wings of the EPR line ~1000 G above and 1000 G below $g = 2.00$. The intrinsic hyperfine couplings to [γ-^{17}O]ATP and [^{17}O]oxalate were in the 8–10-MHz range and somewhat larger than couplings previously observed from $H_2{}^{17}O$ of $[Mn(H_2O)_6]^{2+}$. This work has established conditions for resolving ^{17}O ENDOR features from oxygen ligands which are the most prevalent ligands of Mn^{2+} in biological systems. The spectroscopic resolution and assignments are at a stage of refinement where proton, ^{31}P, and (especially) ^{17}O features can be used as probes for small electronic and structural changes at site I.

The purpose of this work was to probe the vicinity of the enzyme-bound Mn^{2+} which is intimately involved in activating enzyme-catalyzed phosphoryl transfer. In pyruvate kinase the metal sites form the nucleus of a scaffold upon which substrates (ADP and phosphoenolpyruvate) are aligned. Phospho bonds are labilized so that the substrates are in the right proximity for reforming an ATP product and for tautomerizing the pyruvate product from its enol to its keto form. NMR and EPR[1] have given information on exchangeability (Mildvan & Cohn, 1970; Sloan & Mildvan, 1976) and identity (Lodato & Reed, 1987; Buchbinder & Reed, 1990) of metal ligands, and the X-ray structure at 2.6-Å resolution is available for the apo protein (Stuart et al., 1979; Muirhead et al., 1986). The binuclear metal center at the active site of pyruvate kinase offers a good opportunity to examine interactions of the inorganic cations with ligands from the substrate molecules through superhyperfine couplings between paramagnetic metal ions and ligand nuclei. Using ENDOR and

† This work was supported in part by NIH Grant GM 35103 (C.P.S.) and NSF Grants BBS 8711617 (C.P.S.) and GM 35752 (G.H.R.). Acknowledgement is made to the donors of the Petroleum Research Fund, administered by the American Chemical Society, for partial support of this research (PRF Grant No. 19666-AC6).

* To whom correspondence should be addressed at the Department of Chemistry.

‡ Present address: Department of Biological Chemistry, University of California—Davis, Davis, CA 95616-8635.

[1] Abbreviations: CW, continuous wave; ptp, peak to peak; G, gauss; kG, kilogauss; ENDOR, electron nuclear double resonance; EPR, electron paramagnetic resonance; PFSEPR, pulse field sweep EPR; i.d., inside diameter; o.d., outside diameter; RF, radio frequency; ν_p, free proton NMR frequency; $^{31}\nu$, NMR frequency of free ^{31}P; $^{17}\nu$, NMR frequency of free ^{17}O; ν_e, microwave resonance frequency.

0006-2960/93/0432-7799$04.00/0

PFSEPR, we have probed the superhyperfine couplings which characterize ligand nuclei and are sensitive to Mn^{2+}–ligand distances.

The picture of the pyruvate kinase active site which is presently available is one where there are two nearby divalent metals (Gupta et al., 1976; Gupta & Mildvan, 1977; Baek & Nowak, 1982; Muirhead et al., 1986; Lodato & Reed, 1987; Buchbinder & Reed, 1990). We refer to the binding sites for the two nearby divalent metals as site I and site II. Metal ions with larger ionic radii like Mn^{2+} bind at protein-based site I even in the absence of substrate; smaller metals like Mg^{2+} bind to the enzyme at site II as a complex with nucleotide substrate. Site I and site II metals are so close that they can magnetically interact (Gupta, 1977; Lodato & Reed, 1987). A *monovalent* cation is an important cofactor for pyruvate kinase; the enzyme in the presence of K^+ has a ~12-fold higher V_{max} than when Na^+ is present (Nowak & Suelter, 1981). NMR relaxivity of monovalent metal nuclei (Raushel & Villafranca, 1980), EPR of thallium(I) superhyperfine couplings (Lord & Reed, 1987), and ESEEM measurements (Tipton et al., 1989) have indicated physical proximity of the monovalent metal ion binding site to Mn^{2+} at site I.

This study is aimed at the ATP–oxalate complex. Oxalyl phosphate is a substrate for pyruvate kinase, reacting with ADP at the active site to produce oxalate and ATP (Kofron & Reed, 1990). A previous EPR study with ^{17}O-ligated substrate has shown that in this complex ATP's γ-phosphate is simultaneously ligated to both site I and site II metals, and the oxalate is bound through two carboxylic acid oxygens of oxalate to Mn^{2+} at site I (Lodato & Reed, 1987). The complex is thus an enzyme–oxalate–Mn(II)–ATP–Mg(II) complex. Besides the two oxalate oxygens and the γ-phosphate oxygen, the other Mn^{2+} ligands at site I are a water oxygen and probably two oxygens contributed by protein moieties such as the carboxylate of Glu-271 and the main-chain carbonyl groups of Ala-292 or Arg-293 (Muirhead et al., 1986). A schematic of the local environment of Mn^{2+} at site I and of its ENDOR-detected nuclei is shown in Figure 1.

Because $S = {}^5/_2$ Mn^{2+} has long relaxation times in comparison to other metals like iron, the paramagnetic Mn^{2+} gives an EPR spectrum even at room temperature, from which Mn^{2+} hyperfine couplings and the magnitude of zero-field splittings can be determined (Reed & Markham, 1984; Markham et al., 1979). Considerable information on the Mn^{2+} site in pyruvate kinase and other kinases has emerged from EPR studies, especially those at Q-band where line broadening from zero-field splittings is diminished (Reed & Markham, 1984). The identity of phosphate, oxalate, and water oxygen ligands to site I has been determined from EPR line broadening brought on by specific ^{17}O isotopic labeling (Lodato & Reed, 1987; Buchbinder & Reed, 1990). There is a perturbation to the zero-field splittings from Mn^{2+} at site I when one changes the metal at site II, and also a perturbation to the zero-field splittings at site I from altering the monovalent cation (Buchbinder & Reed, 1990). In most cases EPR cannot resolve detailed hyperfine couplings of ligand nuclei like ^{17}O, ^{31}P, or ^1H_2O at Mn^{2+}, and the explanation for Mn^{2+} zero-field splittings is complex (Blume & Orbach, 1961; Sharma et al., 1966). Thus, there is reason for turning to magnetic resonance techniques like ENDOR (Scholes, 1979), PFSEPR (Falkowski et al., 1986), or ESEEM (LoBrutto et al., 1986; Tipton et al., 1989; Larsen et al., 1992) with higher spectral resolution if we want explicit information on electronic structure, ligand identity, or the position of protons which are not resolvable by X-ray and which may not exchange on a time scale amenable to NMR relaxation measurements.

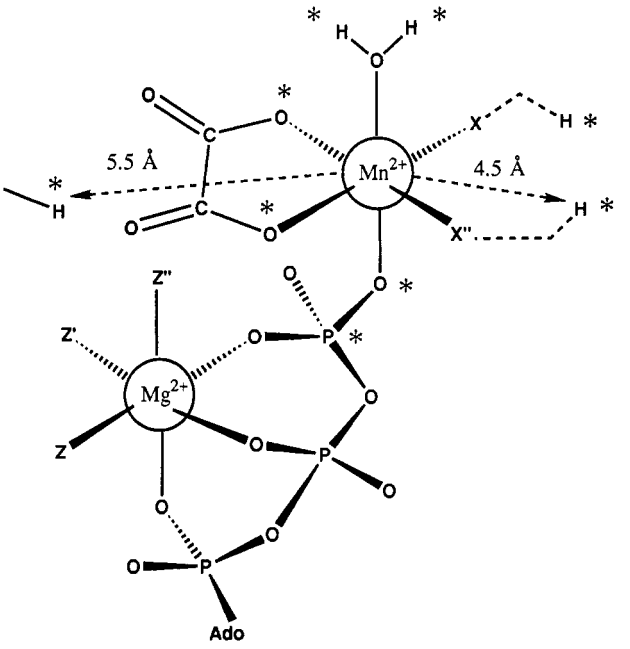

FIGURE 1: A schematic of the Mn^{2+} environs in pyruvate kinase as determined by a combination of information from Lodato and Reed (1987), Buchbinder and Reed (1990), and Muirhead et al. (1986). For this sample, metal I is Mn^{2+} and metal II is Mg^{2+}. The nuclei with asterisks are the ones probed and observed by ENDOR. The exact identity and position of distant, non-water protons with asterisks are somewhat speculative. An exchangeable distant proton, whose ENDOR frequency implied a 5.5-Å distance from Mn^{2+}, is shown as hydrogen-bonded to oxalate; a non-exchangeable proton, whose ENDOR frequency implied a 4.5-Å distant from Mn^{2+}, is shown as part of the liganding protein side chain.

The technique of electron nuclear double resonance (ENDOR) gives great sensitivity in detecting and resolving electron nuclear superhyperfine coupling frequencies to metal ligands (Scholes, 1979). One observes nuclear transitions from their perturbation to the electron spin because RF-induced transitions of those nuclei that are hyperfine coupled to the electron spin alter effective electron spin relaxation rates and lead to an ENDOR-induced change in the EPR signal. The primary information from ENDOR is the ENDOR frequencies; ENDOR intensities can depend in an involved way upon such parameters as temperature, microwave and RF power, and field modulation. The ENDOR technique is more sensitive to large hyperfine couplings and gives the best spectral resolution when first-order hyperfine or Zeeman terms predominate. The complementary technique of ESEEM is most sensitive for detecting weak hyperfine interactions, particularly if hyperfine, quadrupolar, and nuclear Zeeman terms are comparable in magnitude and cause considerable forbidden character in underlying EPR transitions.

At first glance, Mn^{2+} systems with their long relaxation times would seem easy candidates for ENDOR. However, the frozen solution ENDOR spectra can be made complex by couplings to the various M_S electron spin states of the electron spin ${}^5/_2$ manifold and in some cases (such as with water protons) by the anisotropic electron–nuclear hyperfine interaction. A spin ${}^5/_2$ Mn^{2+} ion having magnetic quantum numbers $M_S = \pm{}^1/_2, \pm{}^3/_2$, and $\pm{}^5/_2$ and small zero-field splittings has overlapping electron spin EPR transitions. Even in so simple a system as $[Mn(H_2O)_6]^{2+}$, which yields only proton ENDOR, the result is a set of overlapping ENDOR patterns from proton nuclear coupling to each M_S state. In anticipation of such complexity in enzyme systems, we have

experimentally obtained and theoretically explained frozen solution ENDOR patterns from ^1H (Tan et al., 1993) and ^{17}O (Tan, 1993; X. Tan, M. Bernardo, H. Thomann, and C. P. Scholes, unpublished data, 1993) of H_2O bound to $[Mn(H_2O)_6]^{2+}$. Our preliminary work provided underpinnings for understanding frozen solution ENDOR patterns from ligands to $S = {}^5/_2$ Mn^{2+}, and it has alerted us to complications that we may expect from other types of nuclei coupled to the various electron spin states of Mn^{2+}.

EXPERIMENTAL PROCEDURES

Methods. In doing CW EPR and ENDOR at liquid helium temperatures, we typically monitored the 100-kHz field-modulated dispersion (χ') EPR signal under conditions of adiabatic rapid passage (Portis, 1955; Hyde, 1960). Standard absorption derivative EPR ($d\chi''/dH$) yields well-resolved features where the EPR intensity is changing rapidly with the magnetic field, for example, ^{55}Mn hyperfine features from Mn^{2+} systems near $g = 2.00$. On the other hand, dispersion adiabatic rapid passage yields a spectrum having the appearance of an inverted absorption pattern (not its derivative). The rapid passage signal continues to be found well out in the wings of the Mn^{2+} signal in those regions lacking obvious EPR-detectable hyperfine detail. However, there is considerable hyperfine detail beneath such a rapid passage signal which ENDOR carried out under conditions of rapid passage will resolve. In doing ENDOR, we monitored the RF-induced change in the 100-kHz field-modulated adiabatic rapid passage EPR signal as we swept the frequency of the ENDOR RF field (Tan et al., 1993). Observation of most ENDOR features was done with a 100-kHz modulation of 1–3 G ptp, which we consider as a relatively large modulation field that will enhance larger hyperfine couplings.[2]

For doing PFSEPR, saturating microwave pulses were followed by a field sweep at low monitoring microwave powers, and systematic patterns of transferred saturation, which we have identified with forbidden $\Delta M_S = 1$, $\Delta M_I \neq 0$ EPR transitions, were monitored (Falkowski et al., 1986). PFSEPR is a technically straightforward, low-power pulse technique that uses only the microwave power output of the klystron in our Bruker EPR spectrometer, low-power switching diodes, a simple home-built pulse programmer, and the rapid scan coils that are standard with a Bruker commercial EPR spectrometer.

Materials. Small Mn^{2+} complexes were prepared as frozen glasses in a 1:1 mixture of 50 mM pH 7 Hepes buffer and glycerol (Tan et al., 1993). The deuterated solvent used for these studies was a 1:1 mixture of buffer prepared with 99.9% D_2O and with glycerol-d_3 (where exchangeable OH protons but not the CH protons were deuterated by repeated exchange with D_2O). The glycerol performed as a glass former to prevent aggregation of paramagnetic centers upon freezing and to prevent subsequent unwanted spin–spin interactions between paramagnetic species. In the absence of glycerol there was evidence for aggregation of these small complexes; notably, there was a significant $g = 4$ signal, no rapid passage EPR signals could be obtained, and no CW ENDOR spectra under conditions of rapid passage could be observed.

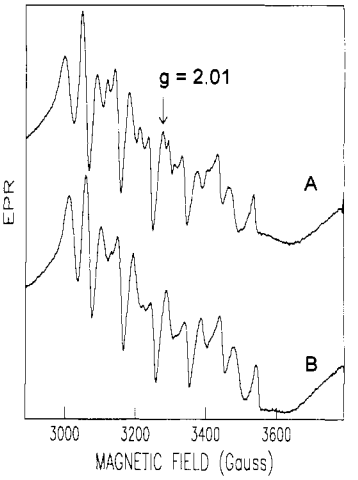

FIGURE 2: A comparison of absorption derivative spectra ($d\chi''/dH$) for pyruvate kinase samples prepared *with* (A) and *without* (B) glycerol. The temperature was 4.2 K and the microwave frequency 9.1928 GHz for (A) and 9.2122 GHz for (B). The 100-kHz modulation was 3 G ptp and microwave power 1 μW. Each spectrum represents four sweeps of 100-s duration over a 1-kG range.

Mn(II)–nucleotide complexes (ATP, CTP, ADP) were prepared in the above solvent and were 1 mM in $MnCl_2$ and 10 mM in nucleotide. In aqueous samples at room temperature such a 10-fold ratio of nucleotide to Mn^{2+} was adequate to eliminate the narrow six-line EPR spectrum of freely tumbling $[Mn(H_2O)_6]^{2+}$. The purpose of these nucleotide model studies was to provide information and conditions about where one might expect ENDOR signals from Mn^{2+}-ligated ^{31}P phosphate.

Pyruvate kinase was prepared from rabbit skeletal muscle according to the method of Tietz and Ochoa (1958). [^{17}O]-Oxalate was prepared by acidic exchange as described previously (Ash, 1982; Lodato & Reed, 1987) and was enriched to 50 ± 2 atom % in ^{17}O. Samples of [γ-^{17}O]ATP were prepared as described by Leyh and Reed (1985) and were enriched to 45 ± 4 atom % in ^{17}O. Lodato and Reed (1987) have shown that additions of $MgCl_2$ to solutions of enzyme, $MnCl_2$, oxalate, and ATP resulted in formation of a dominant complex of the form enzyme–oxalate–Mn(II)–ATP–Mg(II). In our samples the solution contained 50 mM Hepes/KOH, pH 7.5, 55 mM KCl, 2.3 mM enzyme sites, 5.5 mM oxalate, 2.8 mM ATP, 0.82 mM $MnCl_2$, and 6.3 mM $MgCl_2$. These concentrations had previously been determined to result in the formation of a dominant complex of the form enzyme–oxalate–Mn(II)–ATP–Mg(II). Although it was possible to obtain an EPR signal from pyruvate kinase in the absence of glycerol cryoprotectant, the ENDOR signals were much weaker and the EPR lines were slightly broader, indicating aggregation upon freezing.[3] Standard absorption EPR spectra with and without glycerol are shown in parts A and B, respectively, of Figure 2. These spectra are similar, although the narrower EPR lines and slightly greater detail show that cryoprotectant eliminates protein aggregation and freezing-induced distortion of the Mn^{2+} active site.

Samples prepared with [^{17}O]oxalate or with [γ-^{17}O]ATP

[2] A peculiarity of CW ENDOR on the Mn^{2+} samples and on $[Mn(H_2O)_6]^{2+}$ (Tan et al., 1993; Tan, 1993; X. Tan, M. Bernardo, H. Thomann, and C. P. Scholes, unpublished data, 1993) was that they showed a large upward drift in the baseline below about 3 MHz so that we have not shown CW ENDOR spectra below 3 MHz. This upward drift did not appear in the pulsed ENDOR spectra (Tan et al., 1993; Tan, 1993; X. Tan, M. Bernardo, H. Thomann, and C. P. Scholes, unpublished data, 1993).

[3] Many paramagnetic systems aggregate upon freezing, and the spin–spin interactions between paramagnetic centers broaden EPR signals (Leigh & Reed, 1971). In this work such interactions eliminate rapid passage EPR and ENDOR signals. The freezing process in the absence of cryoprotectants may lead to ice crystals and to phases in the immediate protein vicinity where salts are in high concentration (Yang & Brill, 1991). Ice crystals and regions of high ionic strength tend to distort protein structure.

were prepared with deuterated solvent containing 99.9% ^2H_2O and glycerol-d_3 to diminish spectral overlap of ^{17}O ENDOR with exchangeable proton ENDOR, although there was still overlap of nonexchanged protons and ^{17}O ENDOR features. Solutions of the protein were concentrated by vacuum dialysis, diluted 4-fold with buffer in 99% ^2H_2O (pD 7.5) and reconcentrated. This process was repeated four times. Q-band EPR spectra of the samples were identical to those reported previously, including inhomogeneous broadening from [γ-^{17}O]-ATP and [^{17}O]oxalate (Lodato & Reed, 1987).

RESULTS AND DISCUSSION

EPR Results. Because of zero-field splittings, the EPR spectrum of an $S = {}^5/_2$ Mn^{2+} system like pyruvate kinase will be broadened, and the EPR intensity away from $g = 2.00$ will contain significant contributions from $M_S = \pm{}^5/_2$ and $\pm{}^3/_2$ electron spin states. Intense and well-resolved central EPR features as in Figure 2 from the $|-{}^1/_2\rangle \rightarrow |+{}^1/_2\rangle$ EPR transition as observed by first-derivative absorption ($d\chi''/dH$) have shown ^{55}Mn hyperfine structure, higher order effects of zero-field splittings, and at Q-band even broadening from ^{17}O-containing ligands (Lodato & Reed, 1987; Buchbinder & Reed, 1990). However, other EPR transitions of the $S = {}^5/_2$ manifold contribute significantly to the ENDOR spectrum as carried out with adiabatic rapid passage. It is highly significnat for this work that ENDOR, when carried out under conditions of adiabatic rapid passage, samples contributions from these other transitions.

The adiabatic rapid passage signal from $[Mn(H_2O)_6]^{2+}$ is compared in Figure 3A to that of Mn^{2+} from pyruvate kinase in Figure 3B; the pyruvate kinase spectrum is broader because of larger zero-field splittings. Because of its dependence on relaxation times, microwave power, and field modulation frequency and amplitude, an adiabatic rapid passage signal might not be precisely similar to an absorption spectrum such as is measured by spin-echo detection (Tan et al., 1993). However, for $[Mn(H_2O)_6]^{2+}$ there was striking similarity between the spin-echo-detected absorption and the CW-detected dispersion adiabatic rapid passage line shapes.

EPR Theory and Discussion. For $[Mn(H_2O)_6]^{2+}$ Tan et al. (1993) obtained the contributions to the EPR line shape from $\Delta M_S = 1$ EPR transitions. These are the EPR transitions that contribute to the ENDOR features that arise from different M_S spin states. We have done likewise here for Mn^{2+} in pyruvate kinase. The spin Hamiltonian, $\mathcal{H}_e$, which we have used is

$$\mathcal{H}_e = g_e\beta_e\mathbf{H}\cdot\mathbf{S} + D[S_z^2 - 1/3S(S+1)] + E[S_x^2 - S_y^2] + A\mathbf{I}\cdot\mathbf{S} \quad (1)$$

where the first term is the dominant electron Zeeman interaction with an isotropic g-factor of 2.00. The "z" axis is the direction of axial distortion, and the "x" and "y" axes are the directions of rhombic distortion. Thus, the second and third D and E terms in the spin Hamiltonian are, respectively, the tetragonal and rhombic zero-field splitting terms. (A suggestion for the direction of axial distortion could be the pseudo-3-fold axis of symmetry triangulated by the three negative O ligands from oxalate and γ-phosphate of ATP.) The fourth term is an essentially isotropic electron–nuclear hyperfine coupling (of order –90 G) with the $I = {}^5/_2$ nucleus of ^{55}Mn. When the electronic Zeeman term is dominant and zero-field splitting and ^{55}Mn nuclear hyperfine terms provide first-order perturbation, $\Delta M_S = 1$ EPR transitions occur at the magnetic fields, given by eqs 2–6, within the $S = {}^5/_2$ manifold (Reed & Markham, 1984). θ and

$$|-{}^5/_2, m_I\rangle \rightarrow |-{}^3/_2, m_I\rangle \quad (2)$$

$$H = H_0 + Am_I + 2[D(3\cos^2\theta - 1) + 3E\sin^2\theta\cos 2\phi]$$

$$|+{}^3/_2, m_I\rangle \rightarrow |+{}^5/_2, m_I\rangle \quad (3)$$

$$H = H_0 + Am_I - 2[D(3\cos^2\theta - 1) + 3E\sin^2\theta\cos 2\phi]$$

$$|-{}^3/_2, m_I\rangle \rightarrow |-{}^1/_2, m_I\rangle \quad (4)$$

$$H = H_0 + Am_I + [D(3\cos^2\theta - 1) + 3E\sin^2\theta\cos 2\phi]$$

$$|+{}^1/_2, m_I\rangle \rightarrow |+{}^3/_2, m_I\rangle \quad (5)$$

$$H = H_0 + Am_I - [D(3\cos^2\theta - 1) + 3E\sin^2\theta\cos 2\phi]$$

$$|-{}^1/_2, m_I\rangle \rightarrow |-{}^1/_2, m_I\rangle \quad (6)$$

$$H = H_0 + Am_I$$

ϕ denote the polar and the azimuthal angles that the applied magnetic field makes with respect to the zero-field splitting axes. The ^{55}Mn nuclear quantum numbers are $m_I = \pm{}^5/_2$, $\pm{}^3/_2$, and $\pm{}^1/_2$. H_0 is the resonant field at the $g = 2.00$ center of the EPR pattern; H_0 is approximately 3.25 kG for our work. Powder patterns computed for each of the transitions of eqs 2–6, where the magnitudes of D and E were, respectively, 300 and 60 G (Buchbinder & Reed, 1990), are shown in Figure 3C. These simulations were performed for an $S = {}^5/_2$ spin system at $T = 1.8$ K, where the M_S quantum states with the more negative quantum numbers (notably, $M_S = -{}^3/_2$ and $-{}^5/_2$) are the more highly populated and contribute greater integrated EPR intensity.

The purpose of these simulations was to estimate the spread of the overall EPR spectrum and estimate where particular EPR transitions and M_S spin states would predominate. First-order theory was used since the spread of the overall EPR spectrum is predominated by first-order zero-field splitting contributions. We point out that this first-order treatment would be inadequate to predict the exact position of each ^{55}Mn hyperfine line within the set of $|-{}^1/_2\rangle \rightarrow |+{}^1/_2\rangle$ transitions that predominate in the absorption derivative spectra near $g = 2.00$ as shown in Figure 2. In predicting such fine detail, even third-order theory which works well for Q-band spectra (Reed & Markham, 1984) is inadequate for X-band spectra.

The outlying features away from $g = 2.00$ can be effective at selecting subsets of molecules near principle zero-field splitting axes. Regardless of the signs of D and E, the outlying features will be from the $|-{}^5/_2\rangle \rightarrow |-{}^3/_2\rangle$ and the $|{}^3/_2\rangle \rightarrow |{}^5/_2\rangle$ transitions. On the other hand, near $g = 2.00$ all transitions will contribute, and in particular for the $|-1/2\rangle \rightarrow |+1/2\rangle$ transition, all orientations of axes with respect to the static field will be observed. The sign of D in $[Mn(H_2O)_6]^{2+}$ complexes is negative (Tan et al., 1993), and for the simulation of Figure 3C we took both D and E negative (although only the magnitudes of D and E have been determined for pyruvate kinase; Buchbinder & Reed, 1990). In the case of both D and E negative, the EPR intensity at the low end of the spectrum near 2.0 kG predominantly arises from the $|-{}^5/_2\rangle \rightarrow |-{}^3/_2\rangle$ transition, where the magnetic field is near the z axis of the zero-field splitting tensor; the EPR intensity from the $|-{}^5/_2\rangle \rightarrow |-{}^3/_2\rangle$ transition at the high-field end of the spectrum above ~4.2 kG would come from sites where the magnetic field is

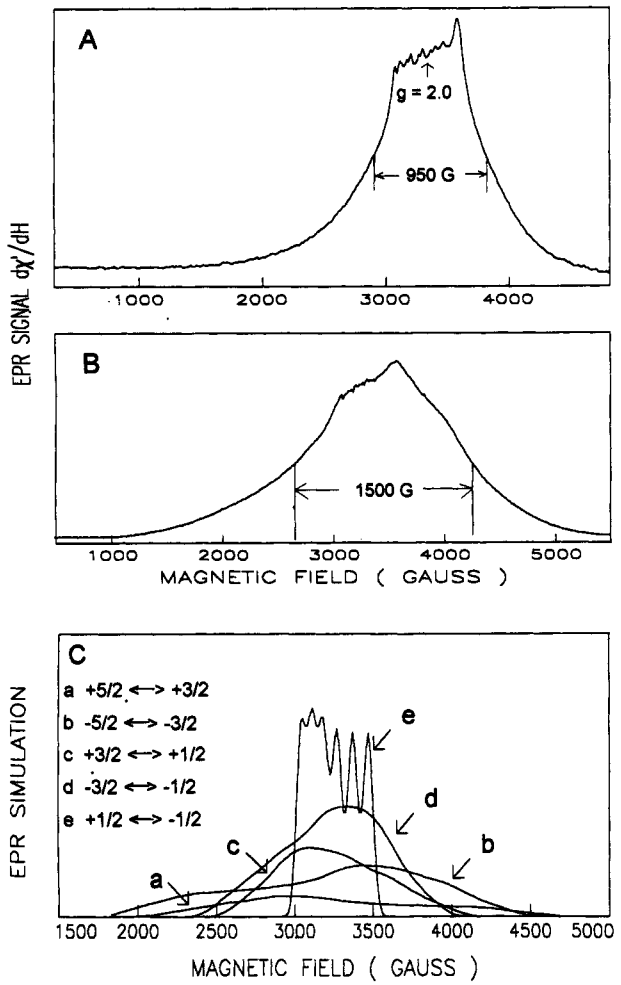

FIGURE 3: (A) Adiabatic rapid passage dispersion signal from $[Mn(H_2O)_6]^{2+}$ in 1:1 glycerol buffer at 2.0 K. Experimental conditions for this measurement were the following: ν_e = 9.132 GHz; field at g = 2.00, 3.26 kG; magnetic field modulation, ~3.0 G ptp; microwave power, ~1 μW. The spectrum is the result of four sweeps of 100-s duration over a 5-kG range. (B) Adiabatic rapid passage dispersion signal from Mn^{2+} in pyruvate kinase from the complex detailed in the Materials as prepared in deuterated solvent. Experimental conditions for this measurement were the following: ν_e = 9.129 GHz; field at g = 2.00, 3.26 kG; magnetic field modulation, ~3.0 G ptp; microwave power, ~1 μW; T = 2.0 K. The spectrum is the result of two sweeps of 200-s duration over a 5-kG range. (C) Simulations of the individual contributions from each $\Delta M_S = 1$ EPR transition where the first-order formulas of eqs 2–6 were used. Parameters used were D = –300 G, E = –60 G, A = –90 G, and H_0 = 3.25 kG after those of Buchbinder and Reed (1990).

near the y axis of the zero-field splitting tensor. If the signs of both D and E were to change, the computed powder patterns for each transition of eqs 2–6 would be reflected through the magnetic field where g = 2.00.

Proton ENDOR Results. In our preliminary study on $[Mn(H_2O)_6]^{2+}$ (Tan et al., 1993), a group of exchangeable water proton ENDOR signals was centered at the free proton frequency (ν_p) when the magnetic field was near g = 2.00. In Figure 4A from $[Mn(H_2O)_6]^{2+}$ these are labeled I, I′; II, II′; and III, III′. In Figure 4A–C, we compare the $[MnH_2O)_6]^{2+}$ spectrum (A) to the pyruvate kinase spectra for protonated (B) and deuterated (C) samples. There is ENDOR evidence for exchangeable water protons in pyruvate kinase consistent with that observed from water of $[Mn(H_2O)_6]^{2+}$, albeit not as intense. ^{31}P and nonexchangeable proton features discussed below became more obvious in the deuterated pyruvate kinase when the overlying exchangeable proton ENDOR signal was eliminated. At a higher field of 3.7 kG outlying exchangeable

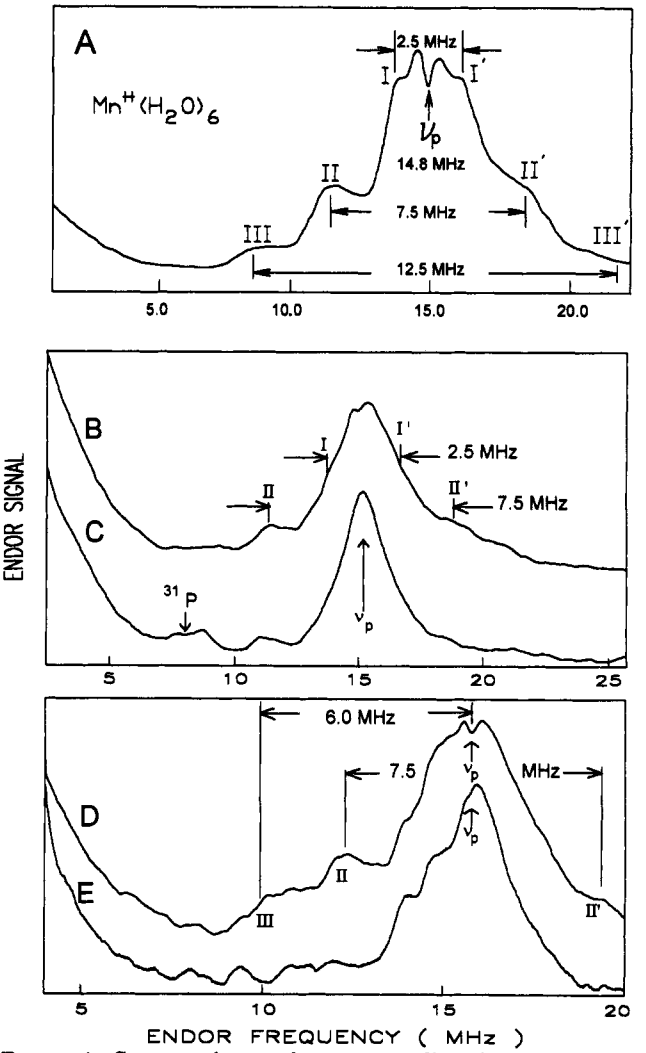

FIGURE 4: Spectra taken to show proton adiabatic rapid passage dispersion ENDOR, primarily from strongly coupled exchangeable water protons. (A) Proton ENDOR spectrum taken from $[Mn(H_2O)_6]^{2+}$ in protonated buffer near g = 2.00. Features labeled I, I′; II, II′; and III, III′ were shown to be exchangeable features from liganding water protons. Conditions for detection of strongly coupled protons were the following: 100-kHz modulation, 1.5 G ptp; H = 3.29 kG; ν_e = 9.153 GHz; microwave power, ~1 μW; T = 1.95 K. This spectrum represents 16 sweeps of 10-s duration into 1024 addresses over a frequency range of approximately 25 MHz. The approximate RF field was 1 G ptp. (B, C) ENDOR spectra from pyruvate kinase in protonated solvent (B) and deuterated solvent (C). These spectra were taken within 250 G of g = 2.00 where all EPR transitions contribute to the ENDOR spectra. Features labeled I, I′ and II, II′ are exchangeable and have the same splittings as the corresponding exchangeable features from $[Mn(H_2O)_6]^{2+}$. Conditions were the following: 100-kHz modulation, 1.0 G ptp; H = 3.49 kG; ν_e = 9.160 GHz; microwave power, ~3 μW; T = 2.1 K. These spectra represent 500 sweeps of 10-s duration into 1024 addresses over a frequency range of approximately 25 MHz. The approximate RF field was 0.5 G ptp. (D, E) ENDOR spectra from pyruvate kinase in protonated solvent (D) and deuterated solvent (E). These spectra were taken at 3.70 kG where contributions of $\pm^5/_2$ and $\pm^3/_2$ electron spin states become more significant. Conditions used were the same as for spectra B and C except the microwave power was ~10 μW, and the spectra represented 128 sweeps of 10-s duration.

proton features were again observed with somewhat higher intensity relative to the features near the free proton frequency, as shown in the comparison of protonated (Figure 4D) and deuterated pyruvate kinase (Figure 4E) at ~3.7 kG.

We made an effort to discover couplings to nonexchangeable protons and exchangeable protons having couplings less than those of Mn^{2+}-liganded water protons. Such features could be useful in probing regions of the active site more distant

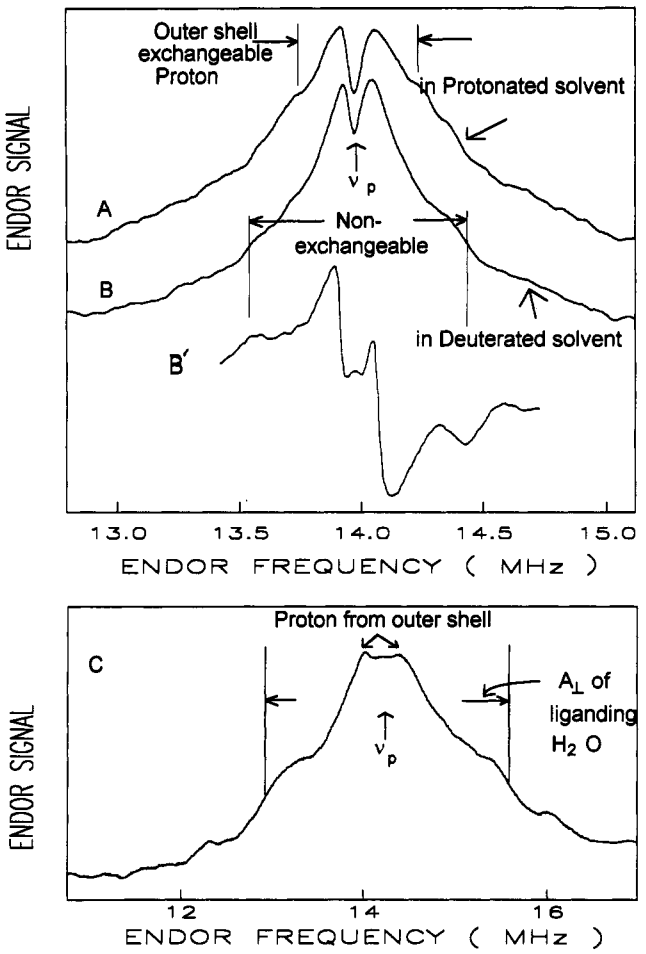

FIGURE 5: Spectra taken to show proton adiabatic rapid passage dispersion ENDOR primarily from *weakly coupled* protons, both exchangeable and nonexchangeable. These spectra were taken near the free proton frequency at $g = 2.00$, $H = 3.28$ kG, and $\nu_e \approx 9.13$ GHz, and with small field modulation to bring out weaker couplings. (A, B) These spectra compare weakly coupled proton spectra from samples prepared in protonated (A) and deuterated (B) solution. The field modulation was ~0.15 G ptp, the microwave power was 10 μW, and $T = 2.1$ K. Each spectrum represents 96 sweeps of 10-s duration over a 3-MHz range about the free proton NMR frequency. The exchangeable feature in spectrum A, whose splitting is much less than that of exchangeable water, has a coupling of 0.45 ± 0.05 MHz. The major nonexchangeable feature had a splitting of 0.85 ± 0.05 MHz. For the deuterated sample of (B) a derivative presentation, denoted as B′, is shown to enhance resolution of features near the free proton frequency. (C) The spectrum from pyruvate kinase in protonated solvent was taken with a field modulation of ~0.6 G ptp. Its purpose is to show both the shoulders from the exchangeable water protons (split by 2.7 MHz) as well as the more weakly coupled exchangeable feature with a splitting of 0.45 MHz. This spectrum represents 96 sweeps of 5-s duration over an 8-MHz range.

than the immediate metal ligands. A comparison of weakly coupled proton ENDOR signals, which are best obtained with small magnetic field modulation, is given in parts A (protonated) and B (deuterated) of Figure 5. The feature in Figure 5B with a splitting of 0.85 ± 0.05 MHz which persisted in the deuterated pyruvate kinase (and was enhanced by taking a derivative as shown in the inset) was clearly from nonexchangeable proton(s). An outer shell exchangeable feature with a coupling of 0.45 ± 0.05 MHz is shown in Figure 5A,C.

Proton ENDOR Discussion. The Mn^{2+} water proton spin Hamiltonian, $\mathcal{H}_{nuc}$, has the form

$$\mathcal{H}n_{uc} = A_\perp I_z S_z + A_\perp (I_x S_x + I_y S_y) - g_n \beta_n \mathbf{H}\cdot\mathbf{I} \qquad (7)$$

where $A_\parallel$ and $A_\perp$ are, respectively, the parallel and perpendicular components of the proton–electron hyperfine tensor, and the spin operators refer to the principal axis direction of this tensor. $g_n = 5.58$ for protons and $\nu_p = g_n \beta_n H$. In frozen solution ENDOR studies on $[Mn(H_2O)_6]^{2+}$, values of $A_\perp = -2.39$ MHz and of $A_\parallel = 7.41$ MHz were experimentally determined from the overall liganding water proton powder ENDOR pattern (Tan et al., 1993). For Mn^{2+}-ligated water the hyperfine tensor largely reflects a proton–Mn^{2+} dipolar interaction whose principal axis directions are parallel and perpendicular to the Mn^{2+}–proton vector (DeBeer et al., 1973). The experimental anisotropic contributions to $A_\perp$ and $A_\parallel$ were, respectively, −3.27 and +6.54 MHz; the contact contribution was 0.88 MHz (Tan et al., 1993). Standard frequency-modulated absorption ENDOR of Mn^{2+} frozen in pH 0.07 perchloric acid has recently provided comparable couplings measured near $g = 2.00$, where water proton couplings to the $M_S = \pm^1/_2$ electron spin states predominate (Sivaraja et al., 1992). A simple point dipolar coupling (discussed below for ^{31}P) between a proton and a paramagnetic Mn^{2+} 2.8 Å from each other would have predicted respective anisotropic contributions of −3.6 and +7.2 MHz to $A_\perp$ and $A_\parallel$.

In frozen solution one obtains a powder ENDOR pattern whose details we have experimentally measured and theoretically simulated for $[Mn(H_2O)_6]^{2+}$ (Tan et al., 1993). In that work we determined that each M_S electron spin state would have effective parallel and perpendicular couplings of $M_S A_\parallel$ and $M_S A_\perp$. In the powder pattern well-resolved extrema occurred with ENDOR frequencies of $\nu_{ENDOR} = |\nu_p - M_S A_\perp|$, and these extrema accounted for features like those in Figure 4A which were assigned as I, I′ (from $M_S = -^1/_2, +^1/_2$); II, II′ (from $M_S = -^3/_2, +^3/_2$); and III, III′ (from $M_S = -^5/_2, +^5/_2$). These features came from orientations where the magnetic field is perpendicular to a water proton–Mn^{2+} direction, and with six water molecules octahedrally arranged in $[Mn(H_2O)_6]^{2+}$ there was ample opportunity for such directions to be sampled in frozen solution, especially near $g = 2.00$. Other weaker shoulders occurred with frequencies given by $\nu_{ENDOR} = |\nu_p - M_S A_\parallel|$.

With pyruvate kinase, proton features having couplings similar to those of water protons of $[Mn(H_2O)_6]^{2+}$ were observed in Figure 4B,D, and these were similarly labeled. At fields away from $g = 2.00$ there were relatively more intense contributions from $\pm^3/_2$ and $\pm^5/_2$ electron spin states whose features are shifted away from ν_p; such features are particularly noticeably from pyruvate kinase in Figure 4D. It is clear that in comparison to $[Mn(H_2O)_6]^{2+}$ the outlying exchangeable proton features are reduced several-fold in intensity in agreement with the smaller number of water ligands for site I Mn^{2+} in pyruvate kinase, but the couplings to the existent liganding water protons are the same as in $[Mn(H_2O)_6]^{2+}$.

Figure 5 was presented with the purpose of showing weakly coupling protons not attached to liganding water. Such protons, occurring ≳4 Å away from Mn^{2+}, would typically be coupled to the electron spin by distance-dependent dipolar coupling having very little covalent contact interaction, and their ENDOR signals may be good probes for small perturbations brought on by substrate, cofactor, inhibitor, or mutagenesis. In a >30 000 molecular weight protein, especially in the vicinity of a paramagnetic metal ion, such protons would not be good candidates for NMR, and if these protons are exchangeable, it is unclear that their exchange rates with bulk water would lead to proton relaxivity (Cohn & Reed, 1982). At $g = 2.00$ where most orientations of a proton hyperfine tensor can be sampled, the largest contribution to

ENDOR of a particular weakly coupled proton will typically come from the $A_\perp$ component of its hyperfine tensor as coupled to the $M_S = \pm^1/_2$ electron spin states. (The perpendicular component can be found in an entire plane of orientations rather than along a single direction like the parallel component.) $A_\perp$ would be given by the simple dipolar formula $A_\perp = -A_{dip} = -g_n\beta_n g_e\beta_e/R^3h$, where R is the Mn^{2+}–proton distance. Therefore, we suspect that the 0.85-MHz coupling to the nonexchangeable proton in Figure 5B would be from a proton ~4.5 Å distant from Mn^{2+}. This proton would be three or four bonds removed from the Mn^{2+}, and it would plausibly be a $-CH_2$ or –CH proton whose carbon was in turn attached to a Mn^{2+}-liganding COOH or backbone carbonyl, respectively, of Glu-271 or Ala-292 or -293 (Muirhead et al., 1986).

The exchangeable proton indicated as the "outer shell" in Figure 5A,C will be at a distance of about 5.5 Å from the Mn^{2+} ion if its hyperfine coupling of –0.45 MHz = $A_\perp$. Such a distance would be consistent with a proton hydrogen-bonded to a carboxyl oxygen four bonds removed from ligation with Mn^{2+}. It has been noted that the amino group of Lys-265 is sufficiently close to the active site to be involved in the catalytic ketonization of bound enolpyruvate (Muirhead et al., 1986). Such a lysine has been suggested by Tipton et al. (1989) as the group having pK = 8.3 (Dougherty & Cleland, 1985) that is responsible for the stereospecific ketonization of enolpyruvate (Kuo & Rose, 1978). An intruiguing hypothesis is that the observed weakly coupled outer shell proton may originate from Lys-265 and be hydrogen bonded to the oxalate inhibitor in the location which it occupies when it provides a proton to enolpyruvate.

^{31}P Phosphate ENDOR and Pulse Field Sweep EPR Results. Mn(II)–nucleotide complexes were first studied to help us in identifying features arising from ^{31}P phosphate. NMR relaxation studies have indicated α, β, and γ coordination of nucleotide phosphates to Mn^{2+} plus three waters of coordination (Sternlicht et al., 1965). On the other hand, a crystal structure has been presented having Mn^{2+} with two liganding ATP's and thus six phosphate ligands (Sabat et al., 1985). It is very likely that in our model nucleotide complexes there will be more than one phosphate ligand per Mn^{2+}. Near g = 2.00 a feature in the 8-MHz region and a partner near 4 MHz were observed from Mn^{2+}–nucleotide complexes in both protonated and deuterated buffer. They were observed in CTP, ATP, and ADP complexes. These features had a splitting of 4.7 ± 0.3 MHz, they were centered at the free ^{31}P NMR frequency ($^{31}\nu$ = 6.03 MHz at 3.5 kG), and they were observed to shift with the field as if centered at $^{31}\nu$. A shoulder somewhat obscured by protons also was evident near 12 MHz. The features are shown for Mn(II)–CTP in Figure 6 and Mn(II)–ATP in Figure 7B. In Figure 6A the ENDOR spectrum from Mn(II)–CTP prepared in protonated solvent also gave evidence for exchangeable protons of water ligated to Mn(II)–CTP, and such protons were similar in their hyperfine couplings to those of $[Mn(H_2O)_6]^{2+}$.

The pyruvate kinase had a feature near 8 MHz in the same general region as found with the nucleotide models. Figure 7A shows this feature labeled ^{31}P as obtained at a magnetic field of 3.2 kG where it had a frequency of 7.4 ± 0.2 MHz. The corresponding feature in Figure 4C was obtained at 3.5 kG, and it had a frequency of 8.2 ± 0.2 MHz. These features did not move with the field like a proton, and they remained even after deuteration. (Because of the sloping baseline at frequencies below 5 MHz, it was difficult to observe any lower frequency partner to this feature in pyruvate kinase.) This

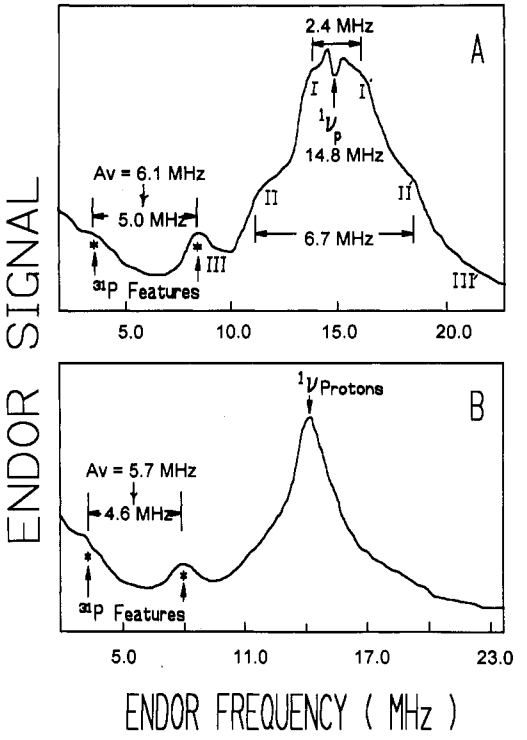

FIGURE 6: A comparison of ENDOR spectra from Mn(II)–CTP model complexes prepared in protonated (A) and deuterated (B) solvent. Conditions were the following: (A) protonated solvent; H = 3.49 kG; $^{31}\nu$ = 5.99 MHz; 100-kHz modulation, 1.5 G ptp; microwaver power, 1 μW; RF intensity, 1 G ptp; ν_e = 9.138 GHz; 32 sweeps of 10-s duration; (B) deuterated solvent; H = 3.33 kG; $^{31}\nu$ = 5.73 MHz; 100-kHz modulation, 1.0 G ptp; microwave power, 1 μW; RF intensity, 0.5 G ptp; ν_e = 9.128 GHz; 64 sweeps of 5-s duration; T = 2.1 K.

~8-MHz signal from pyruvate kinase occurred in a frequency region where ^{31}P features had been seen from nucleotide models. It was weaker than the ^{31}P features of the Mn(II)–nucleotide complexes, and from numerous measurements we estimated it to be ~0.3 MHz lower in frequency than the ^{31}P feature found from nucleotide models.

At low fields where the proton NMR frequency was well removed and where the $|-^5/_2\rangle \rightarrow |-^3/_2\rangle$ EPR transition (see Figure 3C) was likely to predominate, we discovered additional features assignable to ^{31}P. At an outlying field of 2.1 kG a nicely resolved, intense non-proton feature appeared from pyruvate kinase in deuterated solvent at 15.3 ± 0.3 MHz, as shown in Figure 7C. Figure 7D showed no such features for $[Mn(D_2O)_6]^{2+}$, and Figure 7E showed that with a Mn(II)–ATP complex in perdeuterated solvent (containing D_2O and, for this one case, perdeuterated glycerol) there was an ENDOR signal in roughly the same region where the signal from pyruvate kinase was observed, but it was a considerably broader signal. The ENDOR signal at 2.1 kG from the Mn(II)–ATP complex gave the appearance of a powder ENDOR pattern extending from about 14 to 20 MHz.

We used PFSEPR for additional determination of ^{31}P phosphate hyperfine coupling. PFSEPR features arise from forbidden transitions which, as noted by ESEEM researchers, will be particularly prominent if the effective nuclear Zeeman and the hyperfine couplings cancel (Larsen et al., 1992) and will be enhanced by state mixing due to zero-field splittings (Bleaney & Rubins, 1964; Coffino et al., 1992). Near g = 2.00 we observed the PFSEPR features shown in Figure 8 whose splittings, when converted to megahertz, were consistent with the ^{31}P hyperfine couplings determined by ENDOR. The splitting (a – b or a′ – b′) as measured for the Mn(II)–

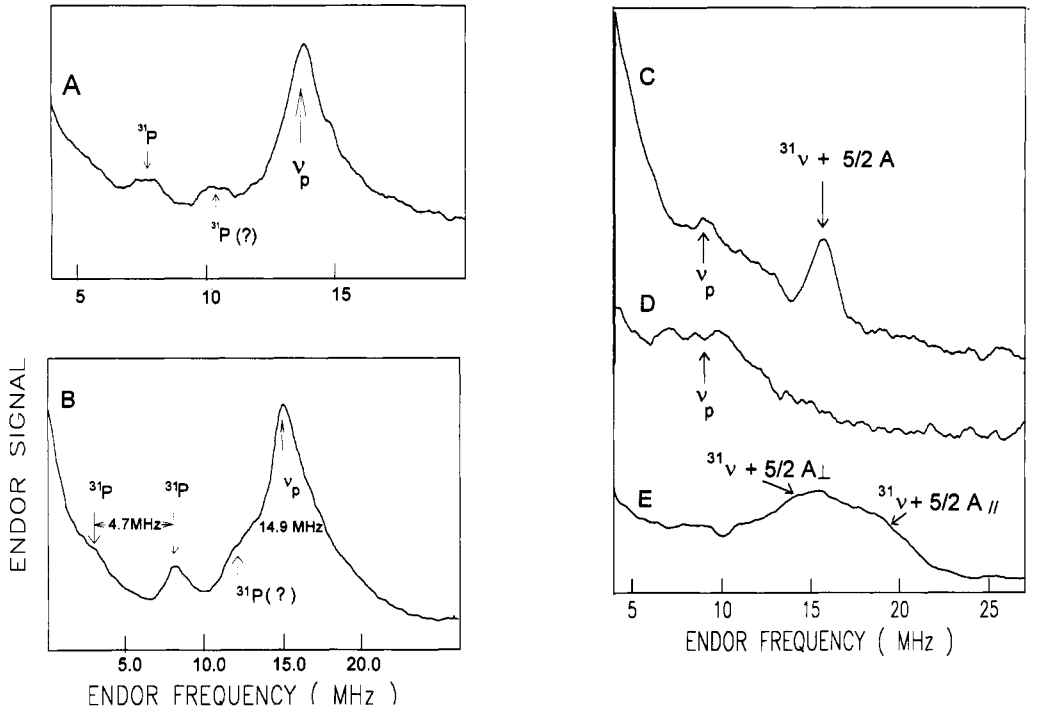

FIGURE 7: Adiabatic rapid passage dispersion ENDOR evidence for ^{31}P coupling in pyruvate kinase and in a Mn(II)–ATP complex. (A) This spectrum was taken from pyruvate kinase in deuterated solvent. It shows ^{31}P features as obtained at fields near $g = 2.00$. Conditions were the following: 100-kHz modulation, 1.0 G ptp; $H = 3.23$ kG; $\nu_e = 9.115$ GHz; microwave power, ~10 μW; $T = 2.1$ K. These spectra represent 128 sweeps of 10-s duration into 1024 addresses over a frequency range of approximately 16 MHz. The approximate RF field was 0.5 G ptp. (B) This spectrum shows ^{31}P phosphate coupling from the Mn(II)–ATP complex in deuterated buffer. Conditions were the following: 100-kHz modulation, 1.0 G ptp; $H = 3.50$ kG; $\nu_e = 9.167$ GHz; microwave power, ~1 μW, $T = 1.95$ K; approximate RF field, 1 G ptp. This spectrum represents 64 sweeps of 5-s duration over a frequency range of 25 MHz. (C) This figure was taken at 2.1 kG from pyruvate kinase in deuterated buffer with the purpose of showing a distinct ^{31}P feature involving ^{31}P coupling to the $M_S = -^5/_2$ state. Conditions were the following: 100 kHz modulation, 1.2 G ptp; $\nu_e = 9.124$ GHz; microwave power, 10 μW; 256 sweeps of 10-s duration over a 25-MHz range. (D) This figure was taken at 2.1 kG from $[Mn(D_2O)_6]^{2+}$ in deuterated buffer for comparison to spectrum C. Conditions are similar to those of spectrum C. (E) This spectrum was taken at 2.1 kG from Mn(II)–ATP in perdeuterated buffer (D_2O and perdeuterated glycerol) with the purpose of showing a distinct ^{31}P feature involving ^{31}P coupling to the $-^5/_2 = M_S$ state. Conditions were the following: 100-kHz modulation, 1.2 G ptp; $\nu_e = 9.124$ GHz; microwave power, 10 μW; 512 sweeps of 10-s duration over a 25-MHz range.

nucleotide models was 4.2 ± 0.3 MHz. Adjacent PFSEPR features overlapped more than ENDOR features, and this overlap made their splittings appear to be slightly less than those measured by ENDOR. A detailed study (see Figure 9) of the splitting of these features from Mn(II)–nucleotide complexes showed that their average frequency undoubtedly tracked the ^{31}P NMR frequency as a function of the magnetic field where they were obtained. The PFSEPR features from pyruvate kinase had less intensity than those from the ^{31}P in the nucleotide models. In the supplementary Figure 1S we show that the resolution of ^{31}P PFSEPR spectral features from pyruvate kinase could be improved by Fourier filtering of the low-frequency components of the spectrum, and the resultant ^{31}P splittings as determined by PFSEPR were ~10% less than the splittings from the ^{31}P phosphate of the nucleotide models. The outcome of the PFSEPR studies is that we confirmed through a technically much simpler method than ENDOR or ESEEM ^{31}P hyperfine couplings that are most certainly unresolved by direct EPR.

^{31}P Phosphate ENDOR and PFSEPR Discussion. ^{31}P is a spin $^1/_2$ nucleus, and in line with our previous work on protons (which are also spin $^1/_2$ nuclei) one expects ^{31}P to have first-order ENDOR frequencies given by

$$\nu_{ENDOR} = |^{31}\nu - M_S A| \quad (8)$$

PFSEPR splittings, δ_H, away from the position of the initial pulse, are similarly related:

$$\delta_H = \pm|^{31}\nu - M_S A|/(g_e\beta_e) \quad (9)$$

Near $g = 2.00$, $M_S = \pm^1/_2$ electron spin states dominate the EPR spectra. We aim this part of the discussion at ^{31}P couplings to the $M_S = \pm 1/2$ electron spin states, although the feature near 12 MHz may arise from ^{31}P coupling to the $M_S = -^3/_2$ electron spin state. According to eq 8, when there is coupling to the $M_S = \pm^1/_2$ spin states, one may expect to see ^{31}P features centered at the ^{31}P NMR frequency and split from each other by the hyperfine coupling A. The ENDOR features from the nucleotide model complexes were split by $A = 4.7 \pm 0.3$ MHz; we take the sign of A as positive in accord with Sternlicht et al. (1965) and Larsen et al. (1992). Since the ATP in frozen solution probably provided a multidentate ligand for Mn(II)–ATP, this coupling may be the average coupling for α-, β-, and γ-phosphates, or it may be dominated by whichever of α, β, or γ more strongly binds to the Mn^{2+}. Because the lower frequency partner predicted at $|^{31}\nu - {}^1/_2A|$ by eq 8 is obscured by the baseline in pyruvate kinase, we have taken the feature observed in the 8-MHz region to be the higher frequency Zeeman partner at $|^{31}\nu + {}^1/_2A|$, and so we obtained a coupling of $A = 4.2 \pm 0.5$ MHz for the phosphate of pyruvate kinase. (Taking only the higher frequency Zeeman partner in computing the hyperfine coupling for the Mn(II)–nucleotide model complexes continued to give $A = 4.7$ MHz for them.) In either pyruvate kinase or the Mn(II)–nucleotide models the ^{31}P hyperfine couplings are of the same order as those determined near $g = 2.00$ by ESEEM measurements of pyruvate kinase (Tipton et al., 1989) and other Mn^{2+} proteins (LoBrutto et al., 1986; Larsen et al., 1992). By comparing couplings measured by ENDOR with each other and by comparing couplings measured by PFSEPR with each other, we determined that ^{31}P couplings measured near $g = 2.00$

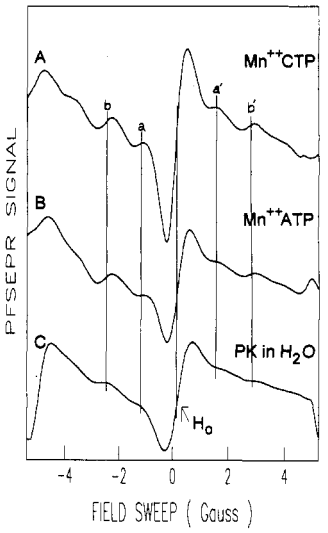

FIGURE 8: Comparison of pulse field sweep EPR spectral evidence for ^{31}P of phosphate hyperfine coupled to Mn^{2+} in complexes of CTP, ATP, and pyruvate kinase in spectra A, B, and C, respectively. These spectra were obtained over a sweep range of ±6 G, sweep time of 20 ms, and 2048 accumulations. Conditions were the following: magnetic field, 3.70 kG; modulation, ~0.1 G ptp; pulse power, ~1 mW; pulse time, 1-ms duration; monitoring power, ~1 μW. The complexes were prepared in protonated media. Feature a is at $-^{31}\nu + {}^{31}A/2$, a′ is at $^{31}\nu - {}^{31}A/2$, b is at $-^{31}\nu - {}^{31}A/2$, and b′ is at $^{31}\nu + {}^{31}A/2$. Because there is considerably more spectral overlap of features in the PFSEPR spectra, the splittings of PFSEPR ^{31}P features appear to be slightly smaller than those measured by ENDOR.

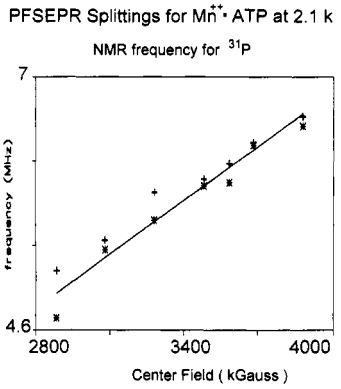

FIGURE 9: Average frequency of PFSEPR features b + a and b′ + a′ plotted as a function of the magnetic field, H_0, where they were obtained. Equation 9 predicts that if these features are from ^{31}P, then this average frequency should be $^{31}\nu = {}^{31}g\beta_n H_0$ (where the nuclear g-value of ^{31}P is 2.24). The theoretical plot is simply a plot of $^{31}\nu$ vs H_0. Experimental points were from field sweeps of ±6.5 G ptp (+) and ±13 G ptp (*). The solid line gives theoretical values.

were smaller for the phosphate of ATP in pyruvate kinase than for the phosphate(s) in the Mn(II)–ATP model.

As pointed out in Figure 3C, EPR features observed at fields well removed from $g = 2.00$ reflect couplings to electron spin states having $|M_S| > {}^1/_2$. Our experience with protons and ^{17}O in $[Mn(H_2O)_6]^{2+}$ was that there is increased enhancement of ENDOR transition probability proportional to $(^{31}\nu - AM_S)^2$, which can be particularly significant for $M_S = -{}^5/_2$ (Tan et al., 1993; Tan, 1993; X. Tan, M. Bernardo, H. Thomann, and C. P. Scholes, unpublished data, 1993). The feature near 15.3 MHz from pyruvate kinase was the clearest and most intense feature that we can assign to ^{31}P, especially since it occurred in a frequency region not overlapped with protons. If the feature at 15.3 ± 0.3 MHz from pyruvate kinase is the result of electron–nuclear coupling to the $M_S = -{}^5/_2$ electron spin state, its ENDOR frequency would be given by eq 8 as $|^{31}\nu + {}^5/_2A|$.[4] Since $^{31}\nu$ is 3.6 MHz at 2.1 kG, the intrinsic hyperfine coupling of this feature is $A = 4.7 \pm 0.1$ MHz, in comparison with the $A = 4.2 \pm 0.5$ MHz coupling to ^{31}P measured in pyruvate kinase near $g = 2.00$. The implication is that we have observed the 15.3-MHz ENDOR feature from ^{31}P because we have monitored the $|-{}^5/_2\rangle \rightarrow |-{}^3/_2\rangle$ electron spin transition.[5] The narrowness of the ENDOR transition near 15.3 MHz, which was obtained far out on the wings of the Mn^{2+} EPR line, revealed that this transition arose from a well-ordered subset of molecules having the magnetic field near an axis of the zero-field splitting tensor and also near a principle ^{31}P hyperfine coupling axis.[4] (If D were negative, that zero-field tensor axis would be the z axis as in Figure 3C.) Given its high resolution, this spectral feature will be a good candidate for future study of perturbation to the phosphate binding site in pyruvate kinase.

The ENDOR pattern was broader near 2.1 kG with the nucleotide models than with the pyruvate kinase, as might be expected if there were several liganding ^{31}P's arranged more randomly in the models. If Figure 7E reflects anisotropy in the ^{31}P hyperfine tensor, then the ^{31}P spectrum stretches from a broad maximum at $|^{31}\nu + {}^5/_2A_\perp| = 13.65 \pm 0.5$ MHz to a shoulder at $|^{31}\nu + {}^5/_2A_\parallel| = 19.1 \pm 1.0$ MHz. Thus, intrinsic ^{31}P couplings of $A_\perp = 4.0 \pm 0.2$ and $A_\parallel = 6.2 \pm 0.4$ can be computed. This $A_\perp$–$A_\parallel$ anisotropy is consistent with a ^{31}P–Mn^{2+} dipolar coupling of $A_d = 0.73 \pm 0.15$ MHz and an isotropic coupling of 4.7 ± 0.3 MHz. Such a ^{31}P–Mn^{2+} dipolar coupling translates into a ^{31}P–Mn^{2+} distance of 3.5 ± 0.2 Å, a distance consistent with the average ^{31}P–Mn^{2+} distance of 3.30 Å reported from the crystal structure of manganese–ATP (Sabat et al., 1985). Even though the ^{31}P of phosphate is farther from Mn^{2+} than the proton of liganding water, its isotropic coupling is much larger than the ~0.8-MHz coupling to water protons (Tan et al., 1993). The implication is that electron spin density is covalently transferred from Mn^{2+} to ^{31}P in a molecular orbital which includes ^{31}P and which interacts through its oxygen with Mn^{2+} in both the Mn(II)–nucleotide models and in pyruvate kinase.

^{17}O ENDOR Results. From recent frozen solution efforts on $[Mn(H_2{}^{17}O)_6]^{2+}$ (Tan, 1993; X. Tan, M. Bernardo, H. Thomann, and C. P. Scholes, unpublished data, 1993) and from previous single crystal ENDOR on this complex doped into a diamagnetic environment (Glotfelty, 1978), we were aware that ^{17}O hyperfine tensor elements for liganding $H_2{}^{17}O$ were in the (–)6 to (–)9 MHz range. We knew that the ENDOR frequencies for ^{17}O coupled to various M_S electron spin states would be given by an equation like eq 10 (below) where the hyperfine term would be the largest, and we had seen that the CW ENDOR frozen solution features of $[Mn(H_2{}^{17}O)_6]^{2+}$ were dominated by the $A_\perp$ component of the hyperfine tensor. On the basis of Q-band EPR line widths, we expected that the hyperfine coupling to [γ-^{17}O]phosphate or [^{17}O]carboxylate ligands would be somewhat (~30%) larger than to an $H_2{}^{17}O$ ligand (Reed & Leyh, 1980). In the previous $[Mn(H_2{}^{16}O)_6]^{2+}$ and $[Mn(H_2{}^{17}O)_6]^{2+}$ studies ENDOR features coupled to electron spin states with higher M_S values gave larger effective couplings and larger ENDOR intensities (Tan et al., 1993; Tan, 1993; X. Tan, M. Bernardo,

[4] In Figure 7C we have indicated the ^{31}P feature as arising from $^{31}\nu + {}^5/_2A$ (rather than $^5/_2A_\perp$ or $^5/_2A_\parallel$) and so have left uncertain for the present which principle hyperfine axis lies near the zero-field splitting axis. Because of the similarity of this value of A and of the $A_\perp$ determined below from the powder-broadened ENDOR of the nucleotide model, we suspect that the A determined from Figure 7C is in fact an $A_\perp$.

[5] The feature from the $M_S = -{}^3/_2$ state would be expected to be weaker, and being closer to the free proton frequency, it is apparently obscured.

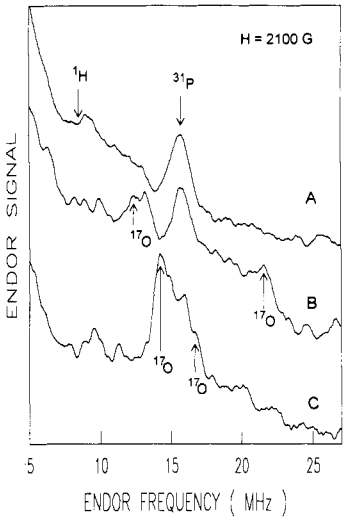

FIGURE 10: Adiabatic rapid passage dispersion ENDOR spectra taken near 2.1 kG to show coupling to ^{17}O in pyruvate kinase prepared either with [γ-^{17}O]ATP or with [^{17}O]oxalate as ligands at site I. Conditions were the following: 100-kHz modulation, ~1.2 G ptp; H = 2.09 kG; ν_e = 9.124 GHz; microwave power, 10 μW; T = 2.1 K. These spectra were taken with sweeps of 10-s duration into 1024 addresses over a frequency range of approximately 25 MHz. The solvent in all cases was D_2O and glycerol-d_3. (A) This is the ENDOR spectrum of pyruvate kinase having *no* ^{17}O ligands and is identical to Figure 7C; the spectrum was taken with 256 sweeps. (B) This ENDOR spectrum is from pyruvate kinase prepared with [γ-^{17}O]ATP; the spectrum was taken with 256 sweeps. (C) This ENDOR spectrum is from pyruvate kinase prepared with [^{17}O]oxalate; the spectrum was taken with 250 sweeps.

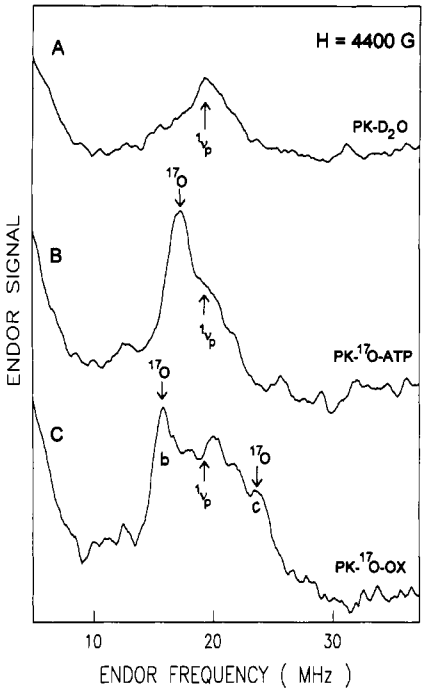

FIGURE 11: Adiabatic rapid passage dispersion ENDOR spectra taken near 4.4 kG to show coupling to ^{17}O in pyruvate kinase prepared either with [γ-^{17}O]ATP or with [^{17}O]oxalate as ligands at site I. Conditions were the following: 100 kHz modulation, ~1.2 G ptp; H = 4.37 kG; ν_e = 9.124 GHz; microwave power, 10 μW; T = 2.1 K. These spectra were taken with sweeps of 10-s duration into 1024 addresses over a frequency range of approximately 35 MHz. The solvent in all cases was D_2O and glycerol-d_3. (A) This is the ENDOR spectrum of pyruvate kinase having *no* ^{17}O ligands; the spectrum was taken with 1000 sweeps. (B) This ENDOR spectrum is from pyruvate kinase prepared with [γ-^{17}O]ATP; the spectrum was taken with 300 sweeps. (C) This ENDOR spectrum is from pyruvate kinase prepared with [^{17}O]oxalate; the spectrum was taken with 686 sweeps.

H. Thomann, and C. P. Scholes, unpublished data, 1993). Experience told us that we would find better resolution and more interpretable information if we looked at outlying EPR features where fewer EPR transitions were present and where the ever-present proton ENDOR might be shifted out of the frequency region of interest. ^{17}O ENDOR in the g = 2 region where electron spins with $M_S = \pm^1/_2$ predominate was not easily observed.

When the magnetic field was near 2.1 kG (1.15 kG below g = 2.00), we identified ^{17}O features as shown in the comparison of part A (having no ^{17}O ligands) with parts B (having [γ-^{17}O]-ATP) and C (having [^{17}O]oxalate) of Figure 10. From the [γ-^{17}O]ATP complex there was a peak near 13.1 ± 0.5 MHz (possibly a double peak) and another weaker shoulder centered at 22 ± 1 MHz. The [^{17}O]oxalate sample gave a peak stretching from 14.7 to 17.7 MHz, appearing to contain several features. These latter features did somewhat overlap with that previously assigned to the ^{31}P feature, but clearly they were not that ^{31}P feature. As shown in Figure 11, taken at the high-field part of the Mn^{2+} adiabatic rapid passage EPR spectrum at 4.4 kG (1.15 kG *above* g = 2), there was an obvious peak in Figure 11B from the [γ-^{17}O]ATP at 16.6 ± 0.3 MHz, and [^{17}O]oxalate features in Figure 11C stretched from 15 to 23 MHz. The relative positions of frequencies from the [γ-^{17}O]ATP feature and the [^{17}O]oxalate features were different from those in Figure 10. There was spectral overlap of ^{17}O and proton features, but there were undoubtedly additional ^{17}O features from both [γ-^{17}O]ATP and [^{17}O]-oxalate.

^{17}O ENDOR Discussion. The ^{17}O hyperfine coupling in $[Mn(H_2{}^{17}O)_6]^{2+}$ was dominated by a Fermi interaction (A_{iso}) of order –7.7 MHz resulting from direct transfer of electron spin to the liganding ^{17}O in the σ Mn^{2+}–O bond. The sign of the ^{17}O hyperfine coupling is negative because of the negative nuclear g-value of ^{17}O, and the A tensor from the single crystal study (Glotfelty, 1978) and from our frozen solution (Tan, 1993; X. Tan, M. Bernardo, H. Thomann, and C. P. Scholes, unpublished data, 1993) ENDOR is in the range $A_\perp$ = –6.5 MHz to $A_\parallel$ = –9.5 MHz. A recent unrestricted Hartree–Fock calculation on $[Mn(H_2O)_6]^{2+}$ predicted 0.21% unpaired electron spin per water oxygen and an isotropic coupling of –6.1 MHz (Sahoo & Das, 1989).

The first-order ENDOR frequencies which include the large hyperfine term and progressively smaller nuclear Zeeman and quadrupolar terms are

$$\nu_{ENDOR} = |M_S A + {}^{17}\nu| \quad (10a)$$

$$\nu_{ENDOR} = |M_S A + {}^{17}\nu \pm 3Q| \quad (10b)$$

$$\nu_{ENDOR} = |M_S A + {}^{17}\nu \pm 6Q| \quad (10c)$$

where A is an effective hyperfine coupling and Q an effective quadrupolar coupling. The ^{17}O nuclear Zeeman interaction is of order 2 MHz, and in single crystals where it could be measured, the quadrupolar splittings were of order 1 MHz (Glotfelty, 1978). In frozen solutions of $[Mn(H_2{}^{17}O)_6]^{2+}$ the quadrupolar couplings were not resolved; the prominent ENDOR features were primarily indicative of $A_\perp$ = –6.5 MHz.

We have given complete first-order expressions in eqs 10a–c that show quadrupolar couplings, but for initially estimating large hyperfine couplings, eq 10a suffices. As may sometimes be the case with ENDOR, not all the predicted spectral features

are seen.[6] However, the evidence which we have gathered is sufficient for us to point out features that originate from ^{17}O and to estimate the hyperfine couplings. Our observations at different magnetic fields give us results whose couplings are consistent with one another and with previous EPR and ENDOR information.[7]

At the field of 2.1 kG the populated spin levels that contribute to the EPR spectrum are $M_S = -3/2$ and $-5/2$, as indicated in Figure 3C and as discussed previously with reference to ^{31}P ENDOR. At this field these transitions are from molecules near a principle zero-field tensor axis, possibly the z direction of the zero-field tensor. In Figure 10B we assign the feature from [γ-^{17}O]ATP at 13.1 MHz to coupling to the $M_S = -3/2$ electron spin state and the feature at 22 MHz to coupling to the $M_S = -5/2$ spin state. Upon application of eq 10a with $^{17}\nu = 1.2$ MHz, the result is $A = -8.0 \pm 0.4$ MHz. Latwesen et al. (1992) reported from liquid-state Q-band EPR a value of 8.1 MHz for $|A_{iso}|$ of Mn-ligated ^{17}O for the γ-phosphate oxygen of GDP in res p21-Mn(II)GDP. That there is agreement with A_{iso} obtained from liquid solution EPR is encouraging, but since our work was carried out in frozen solution where angle selection due to zero-field splitting and hyperfine anisotropy is important, it is not obvious that our measured value of A is in fact A_{iso} (or $A_\perp$ or $A_\parallel$). The [^{17}O]oxalate feature between 14.7 and 17.7 MHz showed more evidence of splitting than the [γ-^{17}O]ATP. Although quadrupolar coupling could be contributing to that splitting, there are not the five quadrupolar features predicted by eqs 10a–c. More straightforward explanations for the splitting are that there is an inequivalence of hyperfine couplings between the two liganding oxalate oxygens or that because of noncolinearity of zero-field tensor axes and [^{17}O]oxalate hyperfine axes, there is still powder averaging. These [^{17}O]oxalate features are most likely also coupled to the $M_S = -3/2$ electron spin state so that the [^{17}O]oxalate hyperfine coupling is in the range –9.0 to –11.0 MHz.[8]

At 4.4 kG as shown in Figure 11 the relative position of the [γ-^{17}O]ATP features and the [^{17}O]oxalate features differed from those in Figure 7 at 2.1 kG. The straightforward explanation is that at 4.4 kG we are probing a set of molecules having a different orientation with respect to the zero-field axis system than the features observed at 2.1 kG. (The interpretation of hyperfine couplings at 4.4 kG is more complicated by spectral overlap of proton and ^{17}O features.) If coupled to the $-3/2$ electron spin state, the γ-^{17}O feature would have a hyperfine coupling of -9.4 ± 0.4 MHz. If coupled to the $M_S = -3/2$ spin state, the [^{17}O]oxalate feature b has an intrinsic coupling of –8.3 MHz, and the [^{17}O]oxalate feature c, if coupled to the $M_S = -5/2$, has an intrinsic coupling of –8.2 MHz.

^{17}O ENDOR features can be uniquely assigned to [γ-^{17}O]ATP and to [^{17}O]oxalate. The ^{17}O couplings are generally in the 8–11-MHz range, which puts them higher than the couplings previously measured for $H_2{}^{17}O$ ligated to Mn^{2+} in $[Mn(H_2O)_6]^{2+}$ (Glotfelty, 1978; Tan, 1993; X. Tan, M. Bernardo, H. Thomann, and C. P. Scholes, unpublished data, 1993) and dominated by covalent spin transfer. It is clear that both [γ-^{17}O]ATP and [^{17}O]oxalate ENDOR features are sufficiently narrow that small changes in them can be identified in future experiments aimed at perturbing the active site I of pyruvate kinase by a change in pH, change in the monovalent activating cation, and change in the site II metal.

CONCLUSIONS

This has been a comprehensive ENDOR study of the liganding environment of Mn^{2+} at site I of pyruvate kinase. It has probed couplings to ^1H, ^{31}P, and ^{17}O of immediate Mn^{2+} ligands and distance-dependent couplings to more distant ^1H. Because a majority of ligands to biological Mn^{2+} are O, this work is significant for having provided for the first time ENDOR hyperfine information on ^{17}O ligands of Mn^{2+} in a protein. The underpinnings are provided here for future study of large classes of kinases where Mn^{2+} at the active site is intimately involved with phosphoryl transfer.

ACKNOWLEDGMENT

We are grateful to Dr. Andrzej Sienkiewicz and to Mr. Harold Taylor for technical help and to Mr. A. Haberl of the State University of New York at Albany Accelerator staff for giving us access to the computers and software there.

SUPPLEMENTARY MATERIAL AVAILABLE

Figure 1S, showing how better resolution of ^{31}P phosphate PFSEPR features can be obtained by Fourier filtering of the low-frequency components (2 pages). Ordering information is given on any current masthead page.

REFERENCES

Abragam, A., & Bleaney, B. (1970) *Electron Paramagnetic Resonance of Transition Ions*, Clarendon Press, Oxford.
Ash, D. E. (1982) Ph.D. Thesis, University of Pennsylvania.
Baek, Y. H., & Nowak, T. (1982) *Arch. Biochem. Biophys. 217*, 491–497.
Bleaney, B., & Rubins, R. S. (1961) *Proc. Phys. Soc. 77*, 103–112.
Blume, M., & Orbach, R. (1961) *Phys. Rev. 127*, 1587–1592.
Buchbinder, J. L., & Reed, G. H. (1990) *Biochemistry 28*, 1799–1806.
Coffino, A. R., & Peisach, J. (1992) *J. Chem. Phys. 97*, 3072–3091.
Cohn, M., & Reed, G. H. (1982) *Annu. Rev. Biochem. 51*, 365–394.
DeBeer, R., DeBoer, W., Van't Hof, C. A., & Van Ormondt, D. (1973) *Acta Crystallogr. B29*, 1473–1480.
Dougherty, T. M., & Cleland, W. W. (1985) *Biochemistry 24*, 5875–5880.
Falkowski, K. M., Scholes, C. P., & Taylor, H. (1986) *J. Magn. Reson. 68*, 453–468.
Glotfelty, H. W. (1978) An ^{17}O ENDOR Study of the Cobalt and Manganese Hydrated Complexes of Some Double Nitrates, Ph.D. Thesis, University of Kansas.
Gupta, R. K., Oesterling, R. M., & Mildvan, A. S. (1976) *Biochemistry 15*, 2881–2887.
Gupta, R. K., & Mildvan, A. S. (1977) *J. Biol. Chem. 252*, 5967–5976.
Gupta, R. K. (1977) *J. Biol. Chem. 252*, 8183–8185.
Hyde, J. S. (1960) *Phys. Rev. 119*, 1483–1492, 1492–1495.
Kuo, D. J., & Rose, I. A. (1978) *J. Am. Chem. Soc. 100*, 6289–6290.

[6] Expected ENDOR features may not have been seen because they are overlapped with more prominent proton features, because they are broadened through powder effects, or, for a case specific to Mn^{2+}, because an M_S electron spin state does not contribute at the field where ENDOR is being observed.

[7] We have found it useful to have previous ^{17}O ENDOR experience with $[Mn(H_2{}^{17}O)_6]^{2+}$ and to have approximate estimates of [γ-^{17}O]ATP and [^{17}O]carboxylate hyperfine couplings, estimated at 3.5 G or 9.8 MHz from EPR line broadenings (Reed & Leyh, 1980).

[8] Although some [^{17}O]oxalate spectra taken near 2.1 kG did show a broad feature in the 22–25-MHz range which would have been the feature coupled to the $M_S = -5/2$ spin state, we have not observed this feature with consistency.

Larsen, R. G., Halkides, C. J., Redfield, A. G., & Singel, D. J. (1992) *J. Am. Chem. Soc. 114*, 9608–9611.
Latwesen, D. G., Poe, M., Leigh, J. S., & Reed, G. H. (1992) *Biochemistry 31*, 4946–4950.
Leigh, J. S., Jr., & Reed, G. H. (1971) *J. Phys. Chem. 26*, 1202–1204.
Leyh, T. S., Goodhart, P. J., Nguyen, A. C., Kenyon, G. L., & Reed, G. H. (1985) *Biochemistry 24*, 308–316.
LoBrutto, R., Smithers, G. W., Reed, G. H., Orme-Johnson, W. H., Tan, S. L., & Leigh, J. S., Jr. (1986) *Biochemistry 25*, 5654–5660.
Lodato, D. T., & Reed, G. H. (1987) *Biochemistry 26*, 2243–2250.
Lord, K. A., & Reed, G. H. (1987) *Inorg. Chem. 26*, 1464–1466.
Kofron, J. L., & Reed, G. H. (1990) *Arch. Biochem. Biophys. 280*, 40–44.
Markham, G. D., Rao, B. D. N., & Reed, G. H. (1979) *J. Magn. Reson. 33*, 595–602.
Mildvan, A. S., Leigh, J. S., Jr., & Cohn, M. (1967) *Biochemistry 6*, 1805–1818.
Mildvan, A. S., & Cohn, M. (1970) *Adv. Enzymol. 33*, 1–70.
Muirhead, H., Clayden, D. A., Barford, D., Lorimer, C. G., Fothergill-Gilmore, L. A., Schlitz, E., & Schmitt, W. (1986) *EMBO J. 5*, 475–481.
Nowak, T., & Suelter, C. (1981) *Mol. Cell. Biochem. 35*, 65–75.
Portis, A. M. (1955) *Phys. Rev. 100*, 1219–1221.
Raushel, F. M., & Villafranca, J. J. (1980) *Biochemistry 19*, 5481–5485.
Reed, G. H., & Leyh, T. S. (1980) *Biochemistry 19*, 5472–5480.
Reed, G. H., & Markham, G. D. (1984) *Biol. Magn. Reson. 6*, 73–142.
Sabat, M., Cini, R., Haromy, T., & Sundaralingam, M. (1985) *Biochemistry 24*, 7827–7833.
Sahoo, N., & Das, T. P. (1989) *J. Chem. Phys. 91*, 7740–7748.
Scholes, C. P. (1979) in *Multiple Electron Resonance Spectroscopy* (Dorio, M. M., & Freed, J. H., Eds.) pp 297–328, Plenum Press, New York.
Sharma, R. R., Das, T. P., & Orbach, R. (1966) *Phys. Rev. 149*, 257–269.
Sivaraja, M., Stouch, T. R., & Dismukes, G. C. (1992) *J. Am. Chem. Soc. 114*, 9600–9603.
Sloan, D. L., & Mildvan, A. S. (1976) *J. Biol. Chem. 251*, 2412–2420.
Sternlicht, H., Shulman, R. G., & Andersen, E. W. (1965) *J. Chem. Phys. 43*, 3123–3132.
Stuart, D. I., Levine, M., Muirhead, H., & Stammers, D. K. (1979) *J. Mol. Biol. 134*, 109–142.
Tan, X., Bernardo, M., Thomann, H., & Scholes, C. P. (1993) *J. Chem. Phys. 98*, 5147–5157.
Tan, X. (1993) Ph.D. Thesis, State University of New York at Albany.
Tipton, P. A., McCracken, J., Cornelius, J. B., & Peisach, J. (1989) *Biochemistry 28*, 5720–5728.
Tietz, A., & Ochoa, S. (1958) *Arch. Biochem. Biophys. 78*, 477–493.
Yang, A.-S., & Brill, A. S. (1991) *Biophys. J. 59*, 1050–1063.